Asian Journal of Chemistry; Vol. 35, No. 8 (2023), 1827-1835

ASIAN JOURNAL OF CHEMISTRY

https://doi.org/10.14233/ajchem.2023.27954

# Fabrication of Eco-friendly Hybrid Active Imidazole based Ionic Liquid Embedded Cadmium Oxide-$TiO_2$ Catalyst for Photoelectrocatalytic and Hydrophobic Properties

J. SUDHALAKSHMI and K. RAJATHI*

P.G. and Research Department of Chemistry, Kalaignar Karunanidhi Government Arts College (Affliated to Thiruvalluvar University), Thiruvannamalai-606603, India

*Corresponding author: E-mail: rajathi_sridhar@rediffmail.com

*Received*: 1 May 2023; *Accepted*: 12 June 2023; *Published online*: 31 July 2023; AJC-21313

In this work, a new and straightforward method for the synthesis of 1-hexyl-3-methyl-2-(2-oxo-ethyl)-3*H*-imidazol-1-ium bromide (HMIB) embedded on CdO-$TiO_2$ (HMIB-CT) hybrid material is reported. The efficiency of the catalytically active material HMIB-CT with nanostructures is entirely depend on the preparation method. The X-ray diffraction patterns revealed that the anatase phase of titanium dioxide results in the formation of well-crystallized CdO and ionic liquid. The optical absorbance spectra demonstrated that the energy gap is diminished from 2.80 to 2.37 eV, which happens due to the presence of ionic liquids. The HR-TEM study shows that the particles are present in spherical shape, while some particles are rod structures with small amount of agglomeration found in imidazole based ionic liquid embedded CdO-$TiO_2$ nanoparticles. The photoluminescence emission results also indicated that ionic liquids efficiently supported and blocked the recombination of charge carriers. A complete demineralization of an organic dye (Trypan blue) under natural sun beam irradiation required for the photocatalytic activity is also accomplished. Moreover, the prepared ionic liquid supported CdO-$TiO_2$ hybrid material shows better electrocatalytic activity upon methanol oxidation (4.89 mA) and super hydrophobic nature by contact angle measurement (112.2º).

**Keywords: Imidazole/CdO-$TiO_2$, Ionic liquids, Nanomaterials, Semiconductors, Photocatalysis.**

## INTRODUCTION

In current days, sustainable technologies are in high demand since producing clean energy is one of the most crucial factors globally. Various types of the liquid wastes are primary risk to humans, animal life and plants [1]. In particular, inorganic and organic dye solutions, which are used in various industries, are highly toxic, non-biodegradable and carcinogenic [2,3]. Therefore, there has been a significant increase in the utilization of synthetic methods to generate various fuels, valuable chemicals and a large quantity of ecologically acceptable molecules in beneficial conditions. In particular, the photocatalytic reactions have been the subject of study into alternative strategies to reduce the environmental pollution.

The photocatalytic technique, which utilizes the advanced nanomaterials, is among the most promising approaches to resolve the water pollution and the energy crisis [4,5]. Over the past decade, heterogeneous photocatalytic degradation of industrial wastes by semiconductors has attracted a lot of attention [6]. Several semiconductors including $TiO_2$ [7,8] CdS-$TiO_2$ [9,10], CdO-ZnO [11], CdS-ZnO [12], $CdWO_4$-ZnO [13] and other materials have been successfully applied as active photocatalysts. $TiO_2$ acted as the better photocatalyst due to its efficiency, minimum cost, free toxicity and high stability. Similarly, CdO is an semiconductor oxide which shows gaining a lot of interest because to its characteristics, such as its broad straight band gap (2.27 eV) and (0.55 eV) tiny indirect band gap and proved as a promising material for better photocatalytic activity [14]. However, hybrid material like CdO-$TiO_2$ is one such material that is useful as a photoactive because it is cheap, long-lasting and has a large enough band gap value, which is necessary for the photo-applications [15,16].

Due to their distinctive qualities like low volatility, non-flammability, strong ion conductivity and thermal and chemical durability, ionic liquids have garnered a lot of attention. It has been found that the high viscosity and lack of surface activity of many ionic liquids [17,18] limits their applicability to a wider range of industries. However, the ionic liquids with high

surface activity have recently attracted the attention of scientists due to their unique physical and chemical properties [19].

Imidazolium ionic liquids have been widely analyzed due to its exclusive physical and chemical properties and potential surface-active applications with high academic and industrial impacts [20,21]. Hence, these ionic liquids are suitable media for nanotechnologies and are also employed as green and sustainable replacement of organic compounds due to their physicochemical properties [22-27]. In this work, we report the synthesis and characterization of 1-hexyl-3-methyl-2-(2-oxo-ethyl)-3*H*-imidazol-1-ium bromide (HMIB) capped CdO-$TiO_2$ hybrid material and investigated its photocatalytic activity of organic dye Trypan blue and antibacterial activity.

## EXPERIMENTAL

The chemicals *viz*. 1-methyl imidazole (MIM), chloroethanol, sodium hydride, acetonitrile and bromohexane were procured and used without additional purification, after the product homogeneity was confirmed by using TLC plates. For the oxidation process, copper wire was also acquired. Trypan blue dye, a synthetic azo dye was procured from Colour Chem company. Titanium isopropoxide (AR grade, Sigma-Aldrich 99.0%) and 2-propanol (spectrochem 99.5%) were also used exactly as received.

### Synthesis of ionic liquids

**1-Hexyl-3-methyl-3*H*-imidazol-1-ium bromide (HMIB-1):** 1-Methyl imidazole (MIM, 0.3 mmol, 24.63 g) and bromohexane (0.3 mmol, 49.52 g) were mixed, stirred vigorously and refluxed at 120 ºC for 48 h in $N_2$ environment. The end-product, a viscous liquid, was dried under vacuum after being cooled to room temperature.

**1-Hexyl-2-(2-hydroxyethyl)-3-methyl-3*H*-imidazol-1-ium bromide (HMIB-2):** Sodium hydride (1.68 g, 0.15 mmol) was added to HMIB-1 (24.5 g, 0.1 mmol) in 50 mL acetonitrile. The solution was supplemented with (8.05 g, 0.1 mol) chloroethanol and continue to agitate for 4 h before being centrifuged to remove any excess NaBr precipitate. The resulting solution was then evaporated to dryness, washed with ether (3 × 20 mL) to get rid of excess alkyl halide and finally the remaining volatiles were removed in vacuum.

**1-Hexyl-3-methyl-2-(2-oxo-ethyl)-3*H*-imidazol-1-ium bromide (HMIB-3):** In a 100 mL beaker, 0.05 mmol of HMIB-2 was added. A hob was used to heat the copper wire. A hot bright red wire was then placed in the compound-containing glass beaker. The same process was repeated for more than 20 times. The dehydrogenation occurs on preheated copper (573 K) when it is submerged in alcoholic compound, resulting in the formation of the corresponding aldehydes. The preliminary and confirmatory tests were assessed and verified the production of aldehyde product (**Scheme-I**). The product was obtained as sticky fluid with high yield (76%). FT-IR (KBr, $cm^{-1}$): 3392, 3143, 2929, 2858, 1625, 1568, 1458 and 1377. $^1$H NMR (400 MHz, $CDCl_3$, ppm): δ 9.73 (t, 1H), 3.67 (d, 2H), 3.64 (s, 3H), 1.28 (m, 2H), 1.34 (m, 2H), 1.4 (m, 2H), 0.97 (t, 3H); $^{13}$C NMR (100 MHz, $CDCl_3$, ppm): δ 199.6, 44.0, 32.3, 30.9, 30.5, 28.0, 26.5, 23.2, 14.0.

**Synthesis of CdO-$TiO_2$ by sol-gel process:** The preparation of CdO-$TiO_2$ composites using the sol-gel technique assisted by ultrasound method. Titanium isopropoxide (12.5 mL) was dissolved in 2-propanol (80 mL), and the remaining volume was made up with distilled water, which was added dropwise and thoroughly stirred. Now, CdO (0.135 g) was added to the aforementioned sol and continue to stir for 2 h and then sonicated for 3 h. A fine and homogenous precipitate was separated, rinsed with deionized water and then allowed to air dry at 100 ºC for 5 h. In a muffle furnace, the product was heated to 400 ºC at a rate of 20 ºC/min for 12 h and then the furnace was allowed to cool at room temperature to obtain a CdO/$TiO_2$ as white powder which constist of 5% CdO content. Similar steps were taken to prepare pure titania ($TiO_2$) without using CdO powder.

**Synthesis of hybrid HMIB-3/CdO-$TiO_2$ (HMIB-CT) material:** In brief, 150 mg of 5 wt.% CdO-$TiO_2$ and 5 mmol of HMIB-3 were added and the mixture was continuously stirred for 1 h followed by the addition of 1 mL of aqueous NaOH dropwise and continued to stir at 80 ºC for varying lengths of time (5 and 20 h). The mixture was then allowed to cool before being rinsed with ethanol and water. After washing, the mixture was centrifuged for 10 min at 3500 rpm to separate the supernatant. A white stable powder of hybrid HMIB/CdO-$TiO_2$ was obtained.

**Characterization:** $^1$H NMR spectra were evaluated using a 400 MHz Varian spectrometer at room temperature with internal TMS as a reference, while a Bruker Alpha-P spectrometer was used for the FTIR analysis. A flux of 100 mL $min^{-1}$ was used during the thermogravimetric analysis (TGA) of the Q50 TA TGA, where the samples (10-15 mg) were heated at a rate of 20 ºC to 800 ºC $min^{-1}$. A JEOL JSM-6701F (FESEM) was used to find out the morphology of the prepared hybrid material, whereas the elemental composition of materials was confirmed by EDS (FEI-QUANTA–FEG 250, equipped with

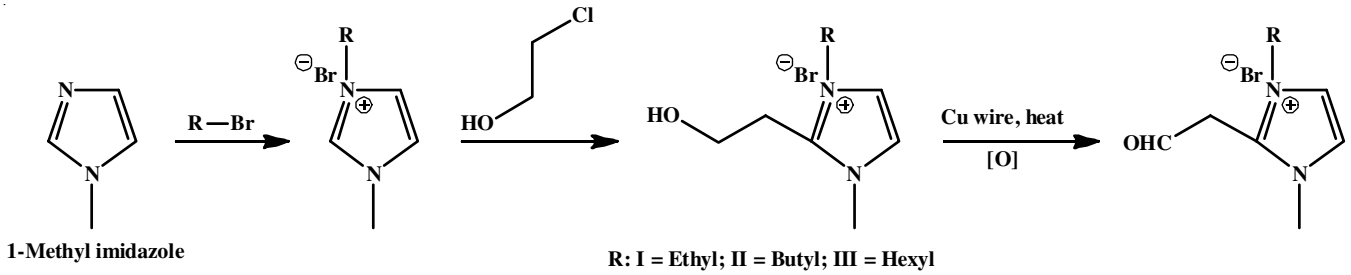


**Scheme-I:** Synthesis of 1-hexyl-3-methyl-2-(2-oxo-ethyl)-3*H*-imidazol-1-ium bromide (HMIB-3)

EDS). TEM analysis was carried out by using Hitachi H-7500. The diffuse reflectance spectra of the prepared samples were recorded in Shimadzu UV 2450 model equipped with an integrating sphere and using powdered $BaSO_4$ as a reference. The photoluminescence (PL) spectrum was recorded using a Perkin-Elmer LS 55 fluorescence spectrometer at room temperature. The cyclic voltammetry (CV) was recorded using CHI660 voltametry instrument, in which the three electrodes make up the cyclic voltammeter *viz*. a platinum wire for the counter electrode, a modified glassy carbon electrode (GCE) for the working electrodes and an Ag/AgCl electrode for the reference electrode, also known as a KCl-saturated electrode. The water contact angle was used to determine the hydrophobicity of the hybrid material coating. To measure the contact angle, a drop-like form analyser (DSA) (Kruss GmbH DE) was employed.

**Photocatalytic degradation:** The photocatalytic studies were conducted during the summer days (April-May) at 11 A.M. to 2 P.M. An average solar light intensity was calculated after every 30 min using The LT Lutron LX-10/A Digital Lux meter. Throughout the studies, the intensity was almost constant. To achieve the both adsorption and desorption process, the dye (trypan blue) and HMIB/CdO-$TiO_2$ mixture were allowed mix vigrously under the magnetic stirring in the dark condition for 30 min. For complete integration of the reaction solution, oxygen was continually supplied to 50 mL of aerated HMIB/CdO-$TiO_2$-dye solution. During the lighting, there was no apparent impact that could have been caused by the temperature. The initial sample was collected *via* dark adsorption and then 2 mL of samples were pipitted at regular intervals. The absorbance of trypan blue dye at 313 nm was measured using a sample solution of 1 mL diluted to 10 mL.

**Hydrophobicity:** The hydrophobicity of the hybrid material is shown by the angle of water contact. Hydrophobic surfaces have a contact angle with water greater than 90º, while the hydrophilic surfaces have an angle of less than 90º. The water contact angle (WCA) of the hybrid material was calculated as the average of these values. The hybrid material coated substrates were sintered in a controlled furnace at 125 ºC for 2 h at a heating rate of 5 ºC $min^{-1}$ to ensure density of the gel network.

**Electrochemical oxidation of methanol:** The working electrode for the methanol oxidation was developed by binding the hybrid material as catalyst on the electrode in nafion. At a scan rate of 50 mV $s^{-1}$, the cyclic voltammograms between +1.0 and -0.1 V were recorded. The reversible hydrogen electrode served as the reference point for all potentials. Following CO adsorption on hybrid material at -0.2 V, the CO stripping voltammetry curves were produced. The electrolyte for the electro-oxidation of methanol was 0.5 M methanol solution in 0.5 M NaOH solution. The anodic peaks in the forward and reverse sweeps were connected to the activity of methanol oxidation.

**Antibacterial studies:** Pathogenic bacterial strains Gram-negative (*Enterobacter cloacae*, *Staphylococus haemolytics*) and Gram-positive (*Bacillus cereus* and *Staphylococcus aureus*) were tested through the well diffusion assay and the results were compared with ciprofloxacin as control. Fresh bacterial cultures in 50 µL were distributed on a prepared plate of Muller Hinton agar. The antibacterial test plates were incubated at 37 ºC for 24 h and the zone of inhibition was quantified in mm [28].

## RESULTS AND DISCUSSION

**Thermal studies:** The TGA analysis further confirms that the compound undergoes two state decomposition on heating at inert atmosphere first decomposition occur at around 25-240 ºC, which is due to the removal of moisture absorbed in the compound. The second decomposition starts at 240 ºC and ended with 380 ºC, which is due to the complete decomposition of prepared ionic liquids (Fig. 1).

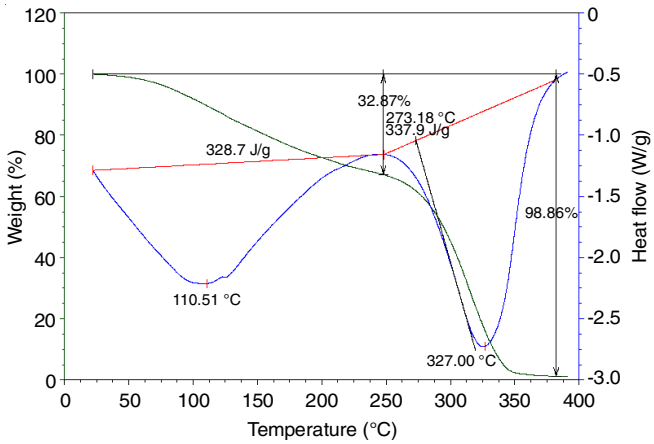


Fig. 1. TGA thermogram of HMIB

**XRD studies:** The XRD spectrum of bare $TiO_2$ and the prepared HMIB/CdO-$TiO_2$ hybrid material are shown in Fig. 2a-b, respectively. The CdO-$TiO_2$ having almost alike 2θ values as $TiO_2$ but intensity differ. In Fig. 2a, the XRD signals precisely

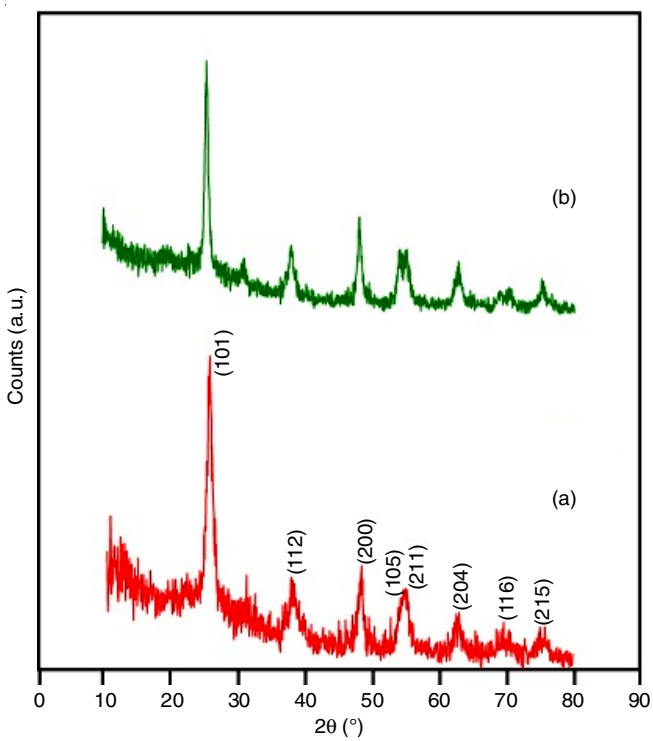


Fig. 2. XRD patterns of (a) bare $TiO_2$ and (b) HMIB/CdO-$TiO_2$

matched with the anatase phase of $TiO_2$. The distinctive peaks of $TiO_2$ at 25.4º, 37.9º, 48.1º, 53.8º, 55.1º, 62.8º, 68.9º, 70.4º and 75.2º are correspond to (102), (113), (200), (106), (212), (205), (117), (220) and (216) diffraction peaks of anatase phase of $TiO_2$ (JCPDS card no. 21-1272) [29]. Fig. 2b exhibits the diffraction peaks of CdO-$TiO_2$, the pattern of CdO-$TiO_2$ do not superimpose with diffraction pattern of bare-$TiO_2$ because of the slight alteration. The average crystallite size of HMIB/CdO-$TiO_2$ was determined using Scherrer's equation and the average crystallite size was found to be 25.2 nm.

**Morphological studies:** As can be shown in Fig. 3, the morphological features of HMIB/CdO-$TiO_2$ hybrid material as revealed by FE-SEM revealed that hydrothermal treatment is a contributing factor to the shape of the prepared material. The HMIB/CdO-$TiO_2$ hybrid material with smooth surfaces and irregular particle shapes were clearly visible in Fig. 3a-c. Moreover, a micro-sponge-like structure and nano-clusters of particles are also clearly visible in Fig. 3b.

The EDS image of HMIB/CdO-$TiO_2$ hybrid material (Fig. 4a) clearly indicate the existence of cadmium, titanium and oxygen. The elemental color mapping (Fig. 4b-e) further confirms the individual atoms (Cd, Ti and O) are present with equivalent ratio in the prepared hybrid material. The TEM was also used to examine the morphology and microstructure of HMIB/CdO-$TiO_2$. The TEM images of HMIB/CdO-$TiO_2$ at various sites and in various photocatalyst dimensions are shown in Fig. 5a-d. The hetero-junctions are formed due to a very close contact between CdO and $TiO_2$ in the composite, as shown by a high-resolution TEM image (Fig. 5c). The majority of the particles in HMIB/CdO-$TiO_2$ hybrid material are under 20 nm in size and have

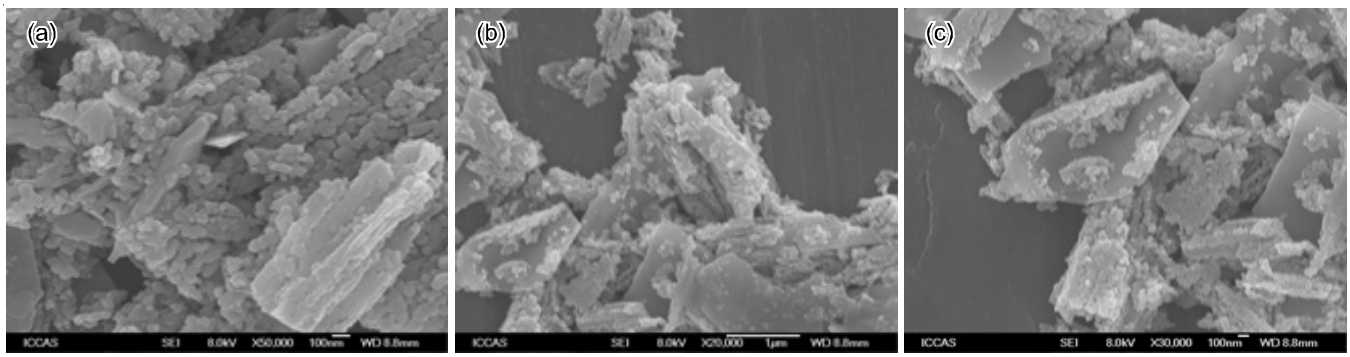


Fig. 3. FE-SEM images of HMIB/CdO-$TiO_2$ at different magnification (a) 100 nm (b) 1 µm and (c) 100 nm

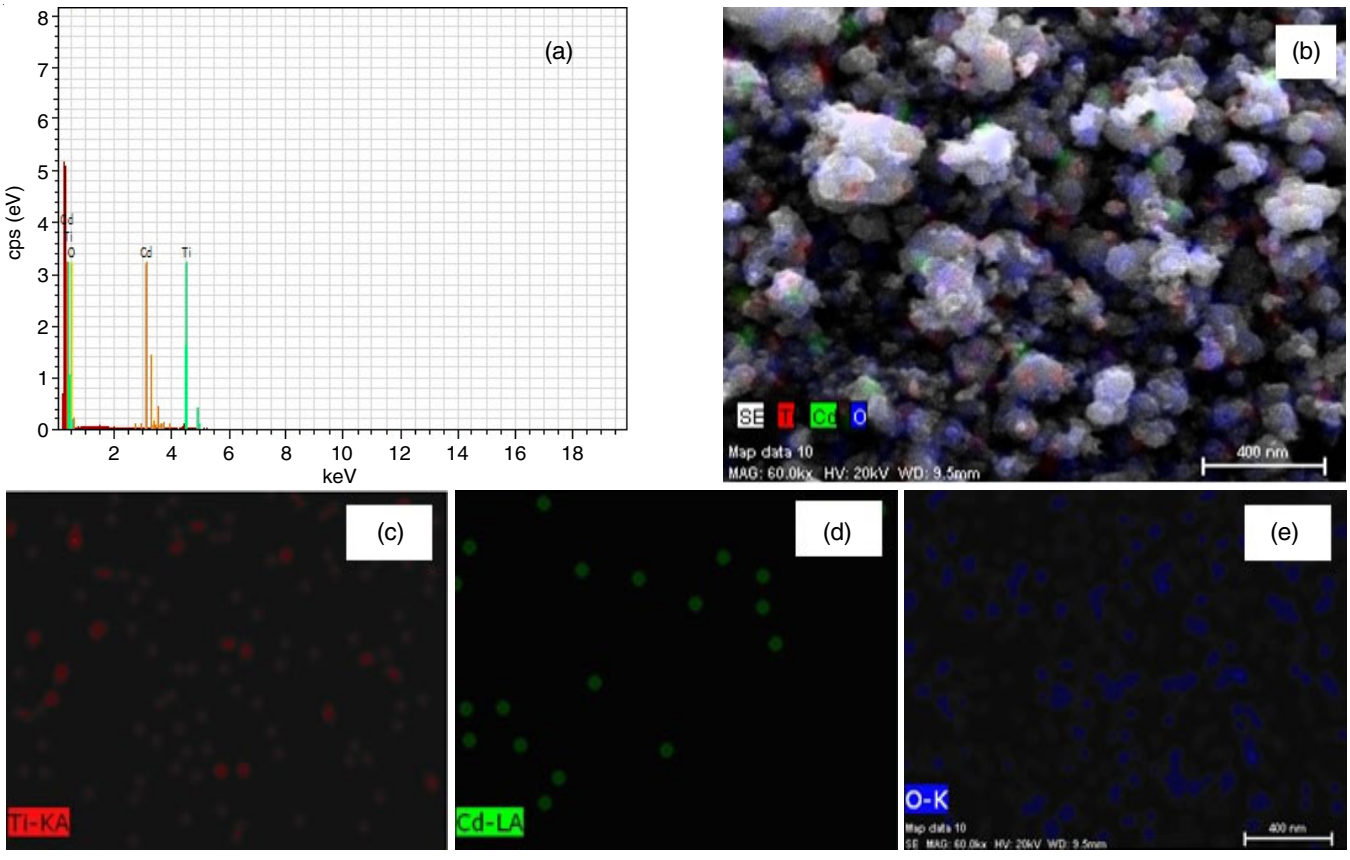


Fig. 4. (a) EDS images and FE-SEM elemental dot (colour) mapping image of (b) HMIB/CdO-$TiO_2$, (c) Ti, (d) Cd and (e) O

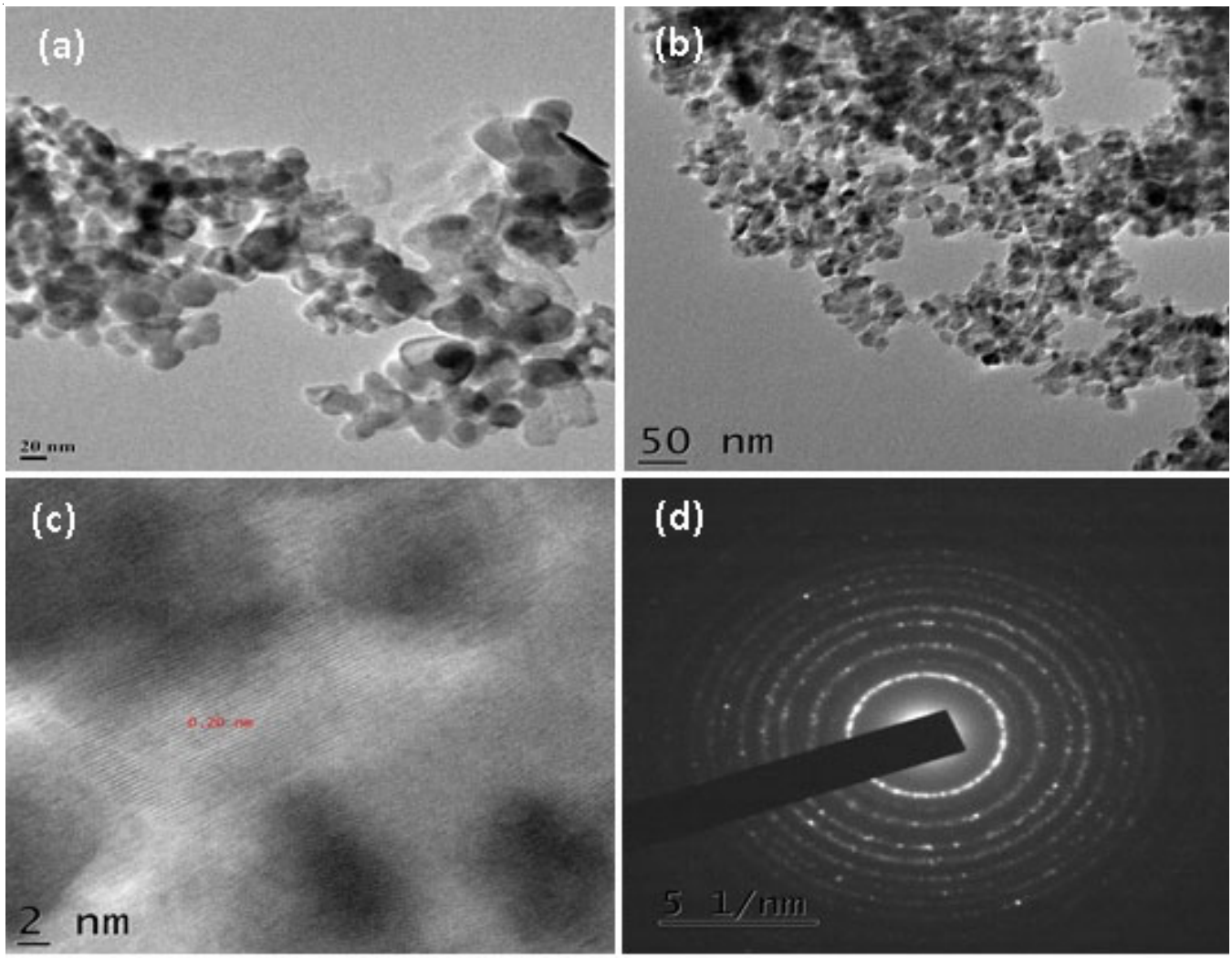


Fig. 5. TEM images of HMIB/CdO-$TiO_2$ (a) 20 nm, (b) 50 nm and (c) HRTEM image of HMIB/CdO-$TiO_2$ (2 nm), (d) SAED pattern

spherical, homogeneous particle shapes. The interplanar spacing in the lattice fringe confirms the tetragonal structure of both CdO and anatase $TiO_2$. The SAED pattern (Fig. 5d) further confirmed their crystallinity and give corresponding plane dots.

The HMIB/CdO-$TiO_2$ X-ray photoelectron spectra is shown in Fig. 6a, whereas the binding energies of titanium, oxygen and cadmium are shown in Figs. 6b-d, respectively. The binding energy peaks for Ti 2p3/2 and Ti 2p1/2 are 459.5 and 465.2 eV, respectively (Fig. 6c) [30]. Normally, the Ti $2p_{3/2}$ line in the case of bare $TiO_2$ sample can be detected at 458.5 eV. The XPS of O1s (Fig. 6d) shows two contributions at 530.7 and 532.7 eV, indicating that the sample contains a diverse range of oxygen species.

## Absorption spectroscopic studies

**Diffuse reflectance spectroscopic (DRS) studies:** The DRS spectrum of HMIB-CT and bare $TiO_2$ are displayed in Fig. 7a-b, respectively. When compared to the bare $TiO_2$, there is a significant absorbance change in the visible area of the DRS spectrum of HMIB-CT. The band gap energy of HMIB-CT is estimated to be 2.37 eV.

**Photoluminescence (PL) studies:** The PL spectra of CdO-$TiO_2$ and HMIB/CdO-$TiO_2$ are exhibited in Fig. 8a-b, respectively. When CdO-$TiO_2$ was embedded in HMIB, the PL emission is not displaced, but the intensity of PL emission decreased, because HMIB successfully prevents electrons from reentering the photocatalyst-generated positively charged holes.

**Degradation studies:** Fig. 9 depicts the rate of trypan blue dye ($1 \times 10^{-4}$ M) degradation under sunlight in the absence and presence of an HMIB/CdO-$TiO_2$ material. Since dye is resistant to self-photolysis, the same experiment conducted in the dark with HMIB-CT showed a decrease in dye concentration (8%). After 60 min in natural sunlight, trypan blue dye degrades to 98% of its original condition using novel hybrid material. Moreover, after 60 min, the degradation rates of CdO, $TiO_2$ and CdO-$TiO_2$ were 24%, 55%, and 68%, respectively. This demonstrates that HMIB-CT is more effective than the other photocatalysts for degrading trypan blue dye.

The effect of trypan blue dye in the pH range of 3-11 and its influence of photomineralization are shown in Fig. 10. When the pH is above or below 7, the degradation efficiency decline. The dissolution of CdO in HMIB-CT may be the cause of the low removal efficiency at the acidic pH ranges. At pH 7, where

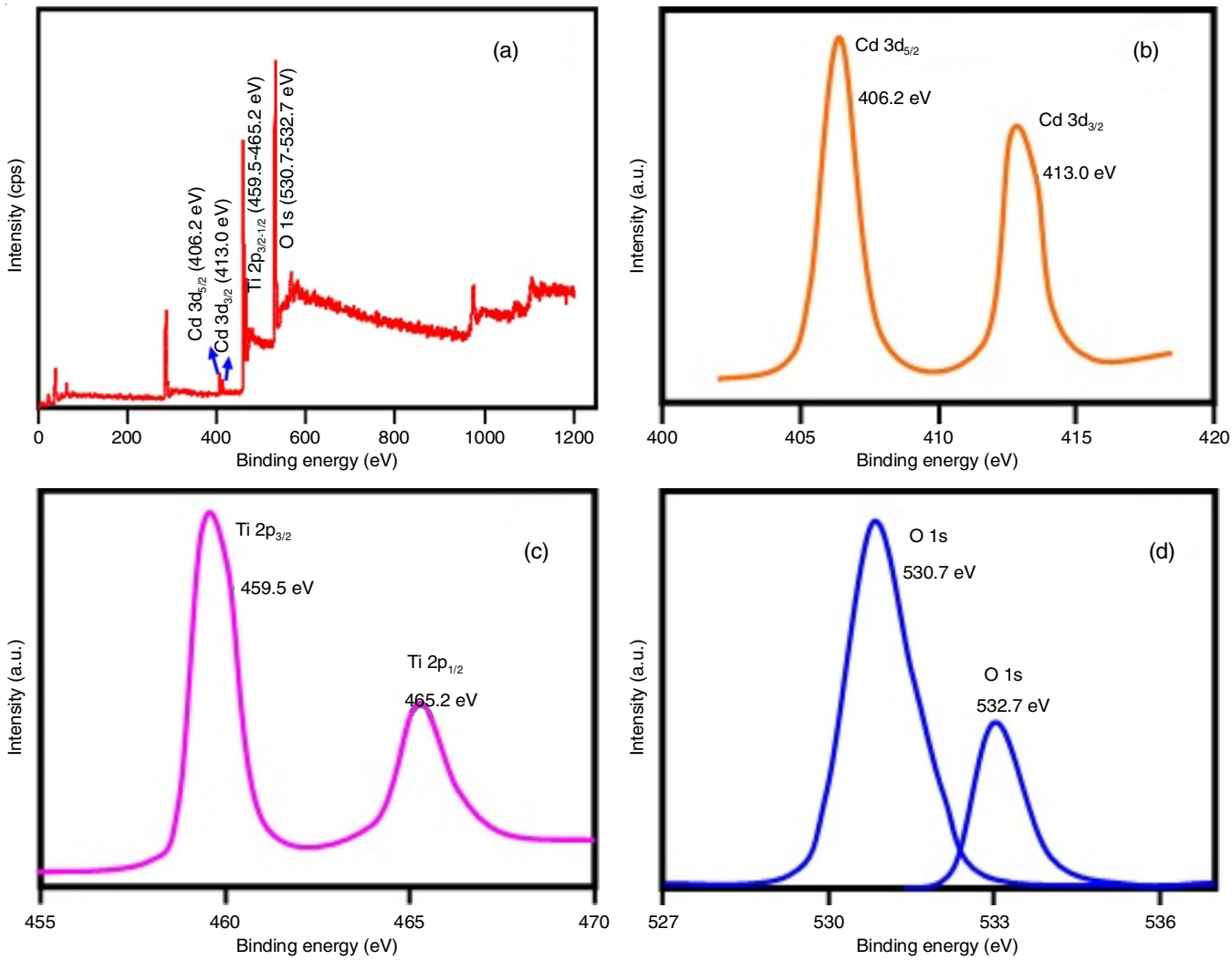


Fig. 6. XPS of HMIB/CdO-$TiO_2$ (a) survey spectrum, (b) Cd 3d peak, (c) Ti 2p peak and (d) O 1s peak

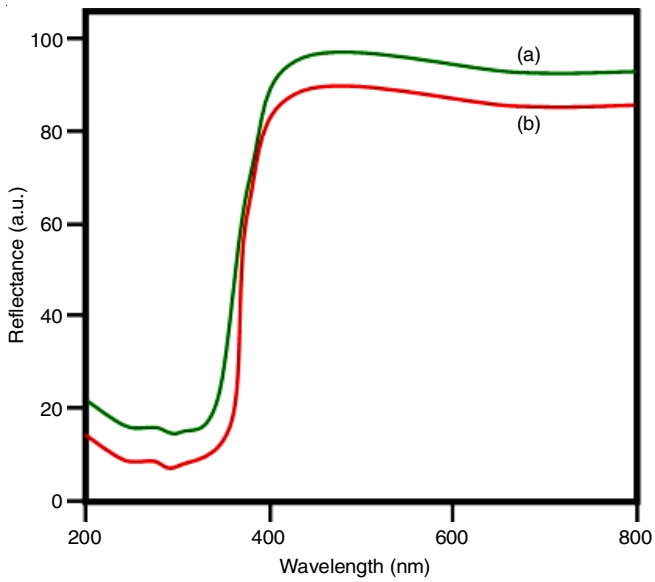


Fig. 7. DRS of (a) bare $TiO_2$ and (b) HMIB/CdO-$TiO_2$

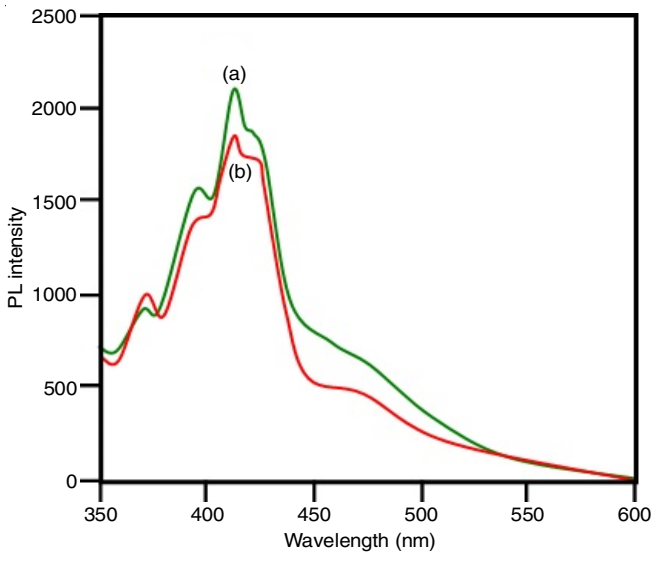


Fig. 8. Photoluminescence spectra of (a) bare $TiO_2$ and (b) HMIB/CdO-$TiO_2$

the adsorption is significant, the deterioration is also more pronounced.

**Degradation mechanism:** An electron passes from the valence band (VB) to the conduction band (CB) and jumps to $TiO_2$'s new energy level when the HMIB/CdO-$TiO_2$ hybrid

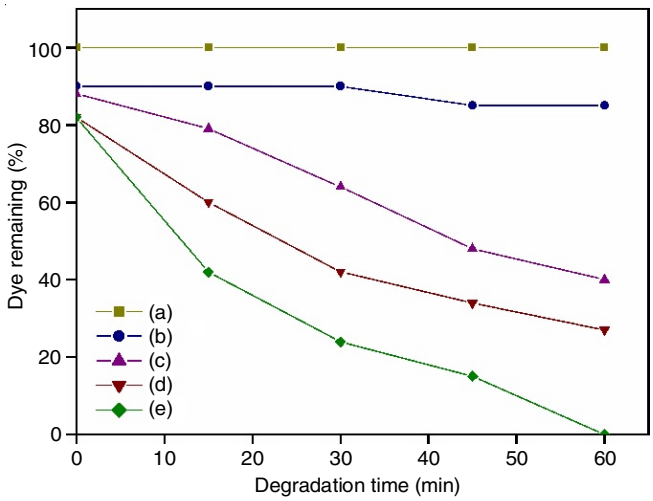


Fig. 9. Photodegradability of trypan blue with different catalysts: (a) without catalyst, (b) bare CdO, (c) bare $TiO_2$, (d) CdO-$TiO_2$ and (e) HMIB/CdO-$TiO_2$

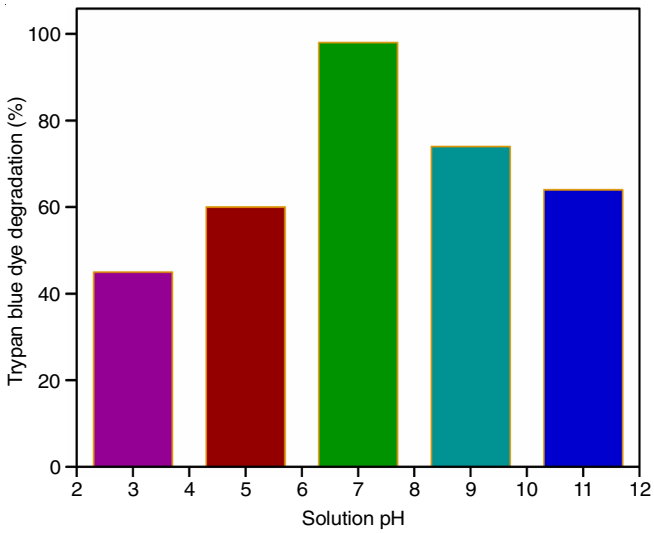


Fig. 10. Effect of pH on degradation of trypan blue dye solution

material absorbs light sources (photons) (eqns. 1-2), leaving a $h^+$ (hole) in the VB. The photogenerated $h^+_{VB}$ can directly oxidize trypan blue dye (eqn. 3) or interact with surface OH groups or chemisorbed water to generate hydroxyl radicals ($^\bullet$OH). In parallel, the photogenerated $e^-_{CB}$ can interact with the ambient $O_2$ that has been absorbed on the surface of the CdO catalyst to produce $^\bullet O_2^-$ (superoxide radicals) (eqn. 2). Finally, the dye molecules continue to interact with these OH and superoxide radicals, resulting in the full photodegradation (eqns. 5-7). Adding dopant HMIB ions to CdO-$TiO_2$ in the current investigation helped to bridge the energy gap, which led to the increased charge carrier separation and resulted in the increased photodegradation of trypan blue dye using HMIB/CdO-$TiO_2$ hybrid material [31]. The mechanism of trypan blue dye photodegradation by HMIB/CdO-$TiO_2$ can be explained as follows:

$$\frac{\text{HMIB}}{\text{CdO}-\text{TiO}_2} + \text{Light } (h\nu) \rightarrow \frac{\text{HMIB}}{\text{Cd}-\text{TiO}_2}(e^- + h^+) \text{ pairs} \quad (1)$$

$$e^-_{CB} + \frac{\text{HMIB}}{\text{CdO}-\text{TiO}_2} \rightarrow \frac{\text{HMIB}}{\text{Cd}-\text{TiO}_2} + {}^\bullet O_2^- \quad (2)$$

$$h^+_{VB}\frac{\text{HMIB}}{\text{CdO}-\text{TiO}_2} + \text{OH (or } H_2O) \rightarrow H^+ + {}^\bullet OH^- \quad (3)$$

$$h^+_{VB}\frac{\text{HMIB}}{\text{CdO}-\text{TiO}_2} + OH^- \rightarrow {}^\bullet OH \quad (4)$$

$$^\bullet OH^- + \text{Dyes (TB dye)} \rightarrow \text{Degraded products } (H_2O + CO_2) \quad (5)$$

$$h^+ + \text{Dyes (TB dye)} \rightarrow \text{Degraded products } (H_2O + CO_2) \quad (6)$$

$$^\bullet O_2^- + \text{Dyes (TB dye)} \rightarrow \text{Degraded products } (H_2O + CO_2) \quad (7)$$

**Reusebility:** The capacity of HMIB-CT to be reused was also examined using the same reaction conditions for trypan blue dye degradation. The hybrid material was thoroughly washed with distilled water and dried for 3 h at 100 ºC in a hot air oven before being employed in a subsequent cycle. The results of trypan blue dye deterioration for four sequential runs are shown in Fig. 11. For 60 min, the cactivity of the hybrid material towards trypan blue dye decay % is 98.0, 97.4, 96.0 and 96.0, respectively. After the second round, the rate at which the efficiency of HMIB-CT hybrid material is deteriorating does not appear to have changed significantly.

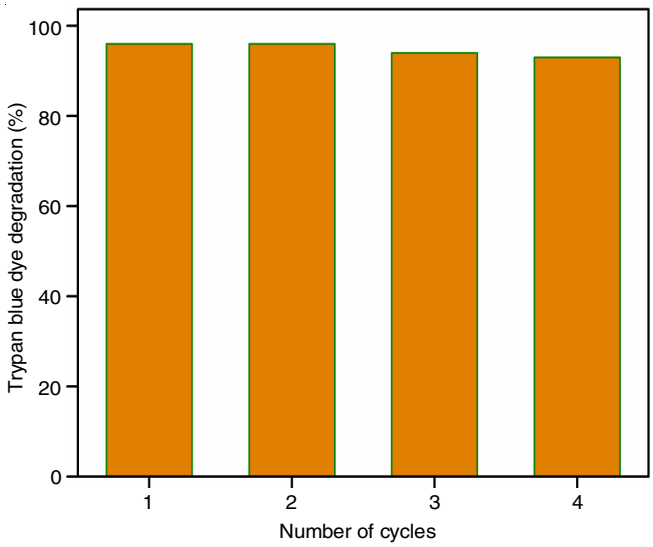


Fig. 11. Reusability of HMIB/CdO-$TiO_2$ on trypan blue dye degradation

**Electrocatalytic oxidation of methanol:** The electrochemical oxidation of up to 20 segments of methanol using CdO-$TiO_2$ is depicted in Fig. 12a using cyclic voltammograms. The current cathodic oxidation peak at 0.02 V (*vs.* Ag/AgCl) in the forward scan and the reduction peak appearing at -0.09V, respectively, indicate the oxidation of methanol and the elimination of CO species adsorbed on the surface of the hybrid material at catalyst. The impact of HMIB on CdO-$TiO_2$ in the oxidation of methanol is clearly explained by the cyclic votammogram of HMIB-CT (Fig. 12b). The current efficiency achieved approximately 4.89 mA, which is three times greater compared with CdO-$TiO_2$ (1.58 mA) and the abrupt anodic peak at 0.10 V caused by methanol oxidation.

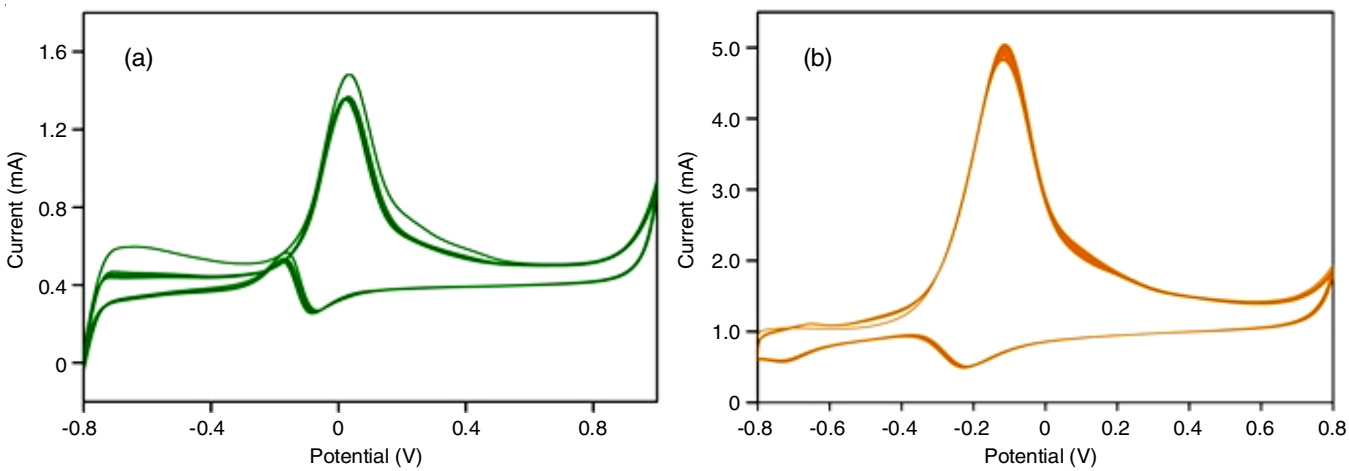


Fig. 12. Cyclic voltammogram of (a) synthesized CdO-$TiO_2$ and (b) HMIB/CdO-$TiO_2$ in $N_2$ and saturated 0.5 M NaOH + 0.5 M $CH_3OH$ solution

**Water contact angle measurements:** Fig. 13 shows a visual representation of water droplets captured on the uncoated and coated HMIB-CT glass slides. Water contact angle (WCA) of 22.6º shows the hydrophilicity nature of uncoated glass slide and WCA increases smoothly on coated slides with TEOS (56.3º), TEOS + CdO-$TiO_2$ (77.5º) and TEOS + HMIB-CT (112.2º). Since the O–Si–O groups in TEOS were modified by HMIB-CT to introduce a rough surface, stable and hydrophobic nature, the surface coating that was prepare using TEOS + HMIB-CT has a greater degree of hydrophobic character. This surface non-wettability of the hybrid material is highly valuable in applications where it is required to clean itself.

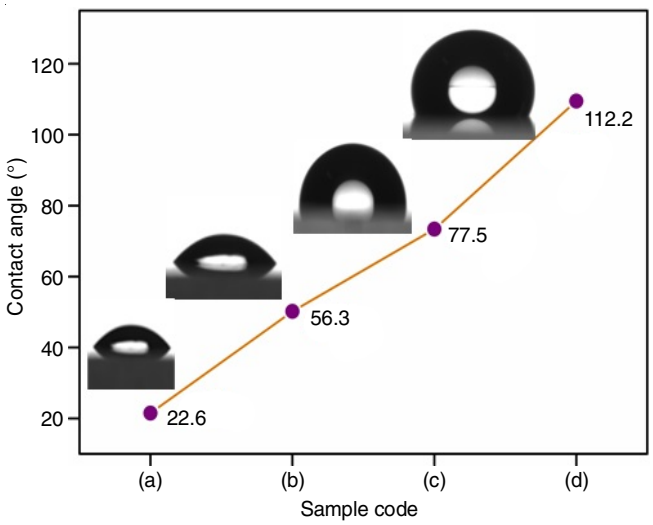


Fig. 13. Water contact angle measurements (a) glass slide (uncoated), (b) TEOS coated glass slide, (c) TEOS with CdO-$TiO_2$ glass slide and (d) TEOS with HMIB/CdO-$TiO_2$ glass slide

**Antibacterial activity:** The antibacterial activity was evaluated by measuring the zone of inhibition in diameter against the studied bacteria *viz*. *B. cereus* and *S. aureus* (Gram positive); *E. cloacae* and *S. haemolytics* (Gram negative). Using the well-diffusion assay, the HMIB-CT shows the zone of inhibition values at 50 µg/mL as 10 mm for *B. cereus* and 9 mm for *S. aureus*, 9 mm for *E. coloacae*, 9 mm for *S. haemolytics* and 9 mm, which is less than standard ciprofloxacin drug (Table-1). These results indicate that a greater concentration of nanoparticles is necessary for the microbiological activity, and it is probable that the lower concentration of individual ions and smaller surface area of the clusters contribute to their reduced antibacterial efficacy.

## Conclusion

In summary, the synthesis and characterization of 1-hexyl-3-methyl-2-(2-oxo-ethyl)-3*H*-imidazol-1-ium bromide (HMIB) embedded on the CdO-$TiO_2$ (HMIB-CT) hybrid material is demonstrated. The average crystallite size of HMIB/CdO-$TiO_2$ calculated as revealed from the XRD analysis was 25.2 nm. The FE-SEM images showed that HMIB/CdO-$TiO_2$ samples consist of fragments with irregular forms and shiny surfaces. Several elements were present as nanocluster and micro-sponge like structure. According to the DRS investigation, the band gap of HMIB-CT is 2.37 eV, which is optimal for absorbing maximum visible light energy. The photocatalytic activity further proves the prepared HMIB-CT hybrid material is highly efficient photocatalysts for the degradation azo dye (trypan blue) under natural sunlight irradiation. The HMIB/CdO-$TiO_2$ produces complete degradation at 60 min. The electrochemical oxidation of methanol using hybrid material explain the ability of conducting current and it produces nearly 4.89 mA. The contact

TABLE-1
ANTIBACTERIAL ANALYSIS RESULT OF HMIB/CdO-$TiO_2$

| Test organism | HMIB (100 µg/mL) | HMIB (50 µg/mL) | Control (Ciprofloxacin) |
|---|---|---|---|
| *Enterobacter cloacae* (Gram-negative) | 11 mm | 10 mm | 15 mm |
| *Staphylococus haemolytics* (Gram-negative) | 10 mm | 9 mm | 16 mm |
| *Bacillus cereus* (Gram-positive) | 11 mm | 9 mm | 17 mm |
| *Staphylococcus aureus* (Gram-positive) | 10 mm | 9 mm | 17 mm |

angle measurement further proves the hydrophobic nature of prepared hybrid material, where HMIB/CdO-$TiO_2$ form contact angle as 110.2º. This super hydrophobic nature may very useful to self cleaning related applications. These results demonstrate the potential of imidazole-based, ionic liquid-supported HMIB/CdO-$TiO_2$ hybrid material for the removal of azo dye as well as other energy and environmental applications.

## CONFLICT OF INTEREST

The authors declare that there is no conflict of interests regarding the publication of this article.

## REFERENCES


1. H. Tong, S. Ouyang, Y. Bi, N. Umezawa, M. Oshikiri and J. Ye, *Adv. Mater.*, **24**, 229 (2012); https://doi.org/10.1002/adma.201102752
2. T. Kamegawa, H. Imai and H. Yamashita, *Bull. Chem. Soc. Jpn.*, **89**, 743 (2016); https://doi.org/10.1246/bcsj.20160080
3. S. Sheik Mydeen, M. Kottaisamy and V.S. Vasantha, *Int. J. Innov. Technol. Exploring Eng.*, **9**, 2278 (2019); https://doi.org/10.35940/ijitee.B7145.129219
4. W. Fan, Q. Zhang and Y. Wang, *Phys. Chem. Chem. Phys.*, **15**, 2632 (2013); https://doi.org/10.1039/c2cp43524a
5. Y. Hong, Y. Jiang, C. Li, W. Fan, X. Yan, M. Yan and W. Shi. *Appl. Catal. B*, **180**, 663 (2016); https://doi.org/10.1016/j.apcatb.2015.06.057
6. H. Wang, X. Li, X. Zhao, C. Li, X. Song, P. Zhang, P. Huo and X. Li, *Chinese J. Catal.*, **43**, 178 (2022); https://doi.org/10.1016/S1872-2067(21)63910-4
7. A. Galinska and J. Walendziewski, *Energy Fuels*, **19**, 1143 (2005); https://doi.org/10.1021/ef0400619
8. M. Anpo and M. Takeuchi, *J. Catal.*, **216**, 505 (2003); https://doi.org/10.1016/S0021-9517(02)00104-5
9. F.-X. Xiao, J. Miao, H.-Y. Wang and B. Liu, *J. Mater. Chem. A Mater. Energy Sustain.*, **1**, 12229 (2013); https://doi.org/10.1039/c3ta12856c
10. S. Manchwari, J. Khatter and R.P. Chauhan, *Inorg. Chem. Commun.*, **146**, 110082 (2022); https://doi.org/10.1016/j.inoche.2022.110082
11. R. Saravanan, H. Shankar, T. Prakash, V. Narayanan, *Mater. Chem. Phys.*, **125**, 277 (2011); https://doi.org/10.1016/j.matchemphys.2010.09.030
12. F. Xu, Y. Yuan, H. Han, D. Wu, Z. Gao and K. Jiang, *CrystEngComm*, **14**, 3615 (2012); https://doi.org/10.1039/c2ce06267d
13. K. Thirumalai, S. Balachandran, K. Selvam and M. Swaminathan, *Emerg. Mater. Res.*, **5**, 264 (2016); https://doi.org/10.1680/jemmr.15.00085
14. S. Balachandran, S.G. Praveen, R. Velmurugan and M. Swaminathan, *RSC Adv.*, **4**, 4353 (2014); https://doi.org/10.1039/C3RA45381B
15. M. Muruganandham and M. Swaminathan, *Sol. Energy Mater. Sol. Cells*, **81**, 439 (2004); https://doi.org/10.1016/j.solmat.2003.11.022
16. C. Burda, Y. Lou, X. Chen, A.C.S. Samia, J. Stout and J.L. Gole, *Nano Lett.*, **3**, 1049 (2003); https://doi.org/10.1021/nl034332o
17. D.N. Kozlov, J. Kiefer, T. Seeger, A.P. Froba and A. Leipertz, *J. Phys. Chem. B*, **115**, 8528 (2011); https://doi.org/10.1021/jp203656z
18. W.L. Hough, M. Smiglak, H. Rodríguez, R.P. Swatloski, S.K. Spear, D.T. Daly, J. Pernak, J.E. Grisel, R.D. Carliss, M.D. Soutullo, J.H. Davis Jr. and R.D. Rogers, *New J. Chem.*, **31**, 1429 (2007); https://doi.org/10.1039/b706677p
19. F. Liu, J. Yu, A.B. Qazi, L. Zhang and X. Liu, *Environ. Sci. Technol.*, **55**, 1419 (2021); https://doi.org/10.1021/acs.est.0c05855
20. N. Nasirpour, M. Mohammadpourfard and S.Z. Heris, *Chem. Eng. Res. Design*, **160**, 264 (2020); https://doi.org/10.1016/j.cherd.2020.06.006
21. L. Wei, L. Wang, Z. Cui, Y. Liu and A. Du, *Molecules*, **28**, 3836 (2023); https://doi.org/10.3390/molecules28093836
22. V.O. Nyamori, M. Gumede and M.D. Bala, *J. Organomet. Chem.*, **695**, 1126 (2010); https://doi.org/10.1016/j.jorganchem.2010.01.019
23. P. Dash, S.M. Miller and R.W.J. Scott, *J. Mol. Catal. Chem.*, **329**, 86 (2010); https://doi.org/10.1016/j.molcata.2010.06.022
24. B.-K. Kim, E.J. Lee, Y. Kang and J.-J. Lee, *J. Ind. Eng. Chem.*, **61**, 388 (2018); https://doi.org/10.1016/j.jiec.2017.12.038
25. B. Xin and J. Hao, *Chem. Soc. Rev.*, **43**, 7171 (2014); https://doi.org/10.1039/C4CS00172A
26. N. Subasree and J.A. Selvi, *Heliyon*, **6**, e03498 (2020); https://doi.org/10.1016/j.heliyon.2020.e03498
27. V. Chauhan, S. Singh and A. Bhadani, *Colloids Surf. A Physicochem. Eng. Asp.*, **395**, 1 (2012); https://doi.org/10.1016/j.colsurfa.2011.11.022
28. R.J.V. Michael, B. Sambandam, T. Muthukumar, M.J. Umapathy and P.T. Manoharan, *Phys. Chem. Chem. Phys.*, **16**, 8541 (2014); https://doi.org/10.1039/c4cp00169a
29. L.C. Sim, K.H. Leong, S. Ibrahim and P. Saravanan, *J. Mater. Chem. A Mater. Energy Sustain.*, **2**, 5315 (2014); https://doi.org/10.1039/C3TA14857B
30. P. Zhou, Z. Le, Y. Xie, J. Fang and J. Xu, *J. Alloys Compd.*, **692**, 170 (2016); https://doi.org/10.1016/j.jallcom.2016.09.039
31. K. Manjunath, L.S. Reddy Yadav, T. Jayalakshmi, V. Reddy, H. Rajanaika and G. Nagaraju, *J. Mater. Res. Technol.*, **7**, 7 (2018); https://doi.org/10.1016/j.jmrt.2017.02.001